Progress In Electromagnetics Research, *PIER 14, 1–36, 1996*

P0LARIMETRIC SCATTERING THEORY FOR HIGH SLOPE ROUGH SURFACES

A. Ishimaru, C. Le, Y. Kuga, L. A. Sengers, and T. K. Chan

1. Introduction

Electromagnetic scattering by rough surfaces is important in several disciplines including geophysical remote sensing, ocean acoustics, surface optics, and ultrasound imaging of biological media [1–24]. For surfaces with small rms height, the conventional perturbation theory is applicable while for surfaces with large radii of curvature, Kirchhoff theory gives good solutions. In recent years, several improved theories have been proposed to extend the range of validity of surface parameters, and numerical simulation studies have been reported [5–24]. This paper presents a theory based on the first and second Kirchhoff approximations with angular and propagation shadowing [16–21]. Its range of validity is considerably larger than most of the previous theories using Kirchhoff approximations, and it is applicable to rough surfaces with high slopes of order unity. There are two important points in the theory [17,18]. The first is that the Green's function is expressed by the Fourier transform in the y - z plane transverse to the propagation direction x, rather than the usual Fourier transform in the x - y plane parallel to the average rough surface. The wave on the surface is then divided into the positive traveling and the negative traveling waves. The advantage of this technique is that there is no longer a need for the absolute values $|z_1 - z_2|$ of the difference heights ($z_1 - z_2$), and therefore large height variations and large slopes can be incorporated into the statistical moment calculations. The second important point is that for second-order scattering we make use of angular and propagation shadowing functions. This, in essence, takes care of the multiple scattering beyond second-order scattering. These two features, the Fourier expansion in the y - z plane and the shadowing corrections, make possible the expansion of the range of validity of the theory beyond those for conventional techniques.

The theory gives an analytical expression for the complete 4×4 cross section Mueller matrix. It consists of the first-order Kirchhoff term which has been obtained previously and the second-order Kirchhoff terms including shadowing corrections, which we obtained recently. The second-order terms include the ladder term and the cyclic term, and the cyclic term gives rise to enhanced backscattering.

The second-order terms are given by quadruple integrals. These integrals are then reduced to numerically manageable double integrals. Numerical examples are shown for the cases of ($\sigma = 1\lambda$, $l = 4\lambda$), ($\sigma = 1\lambda$, $l = 3\lambda$),($\sigma = 1\lambda$, $l = 2\lambda$), and ($\sigma = 1\lambda$, $l = 1.4\lambda$) where σ is the rms height and l is the correlation distance. Co-polarized and cross-polarized components are calculated and compared with millimeter wave experimental data, showing good agreement.

The range of validity of the present theory may be seen in Fig. 1. The present theory includes the first- and second-order Kirchhoff approximations with shadowing corrections and is applicable to the region (E) where backscattering enhancement takes place. There have been many attempts to extend the region of validity of conventional perturbation theory (FP) and Kirchhoff (KA) theory. For example, phase perturbation theory (PP) attempts to bridge the region between the perturbation and Kirchhoff theories. More recent work [14] extends the region of validity of (PP) with computational advantages, while the unified perturbation method (UPM) [24] covers a wider range of slopes than the conventional Kirchhoff approximation. The present theory is directed to the region of high slopes on the order of 0.5 to 1.5 which is not covered by existing theories.

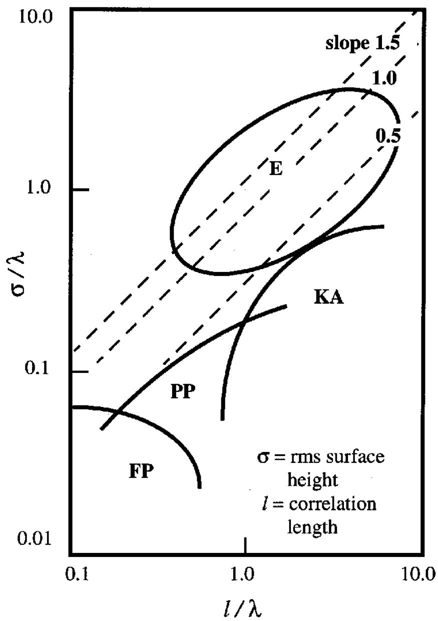

Figure 1. Range of validity of the present theory. The present theory is valid in the region (E) where backscattering enhancement takes place. (KA) and (FP) are where Kirchhoff approximation and the field perturbation theory are valid, respectively. (PP) is where phase perturbation theory is valid.

2. Formulation of the Mueller Matrix [M] and the Cross Section Mueller Matrix $[\sigma]$

Let us consider the wave scattered from two-dimensional rough surfaces between two media, Figure 2. The scattered wave at the observation point $\overline{r}$ is given by

$$\overline{E}(\overline{r}) = \nabla \times \nabla \times \overline{\pi} + i\omega\mu\nabla \times \overline{\pi}_m \tag{1}$$

where

$$\overline{\pi} = \frac{i}{\omega\epsilon_0}\int \hat{n}_1 \times \overline{H}_1 g dS_1$$
$$\overline{\pi}_m = \frac{i}{\omega\mu}\int \overline{E}_1 \times \hat{n}_1 g dS_1$$
$$g = \frac{\exp\left[ik\left|\overline{r}_1 - \overline{r}_2\right|\right]}{4\pi\left|\overline{r}_1 - \overline{r}_2\right|}$$

$\overline{E}_1$ and $\overline{H}_1$ are the surface fields at $\overline{r}_1$. If we write

$$\begin{aligned}\overline{E}_1 &= \overline{E}_{1i} + \overline{E}_{1s}\\ \overline{H}_1 &= \overline{H}_{1i} + \overline{H}_{1s}\end{aligned} \tag{2}$$

where $(\overline{E}_{1i}, \overline{H}_{1i})$ are the incident fields at $\overline{r}_1$, then the contribution to (1) from $(\overline{E}_{1i}, \overline{H}_{1i})$ is zero, and therefore we can write (1) using $\overline{E}_{1s}$ and $\overline{H}_{1s}$ in place of $\overline{E}_1$ and $\overline{H}_1$.

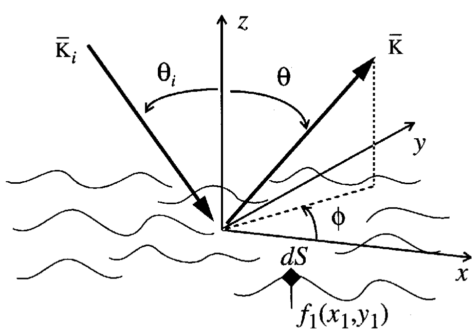

Figure 2. Rough surface is given by $z = f_1(x_1, y_1)$, and the surface element dS is at $\overline{r}_1 = x_1\hat{x} + y_1\hat{y} + f_1(x_1, y_1)\hat{z}$. $\overline{K_i} = k\hat{i}$ and $\overline{K} = k\hat{o}$.

The first-order Kirchhoff approximation (KA-1) for $\overline{E}_{1s}$ is obtained by using the incident wave for $\overline{E}_{1i}(\overline{E}_{1i} = \overline{E}_1)$ and calculating $\overline{E}_{1s}$ from the local reflection coefficient. The second-order Kirchhoff approximation (KA-2) is obtained by using the Kirchhoff approximating for the scattered wave from the surface. If we consider the very rough surfaces, we can make further approximations using the geometric optics approximation and choosing the normal vectors $\hat{n}_1$ and $\hat{n}_2$ at the stationary phase points. See Figure 3.

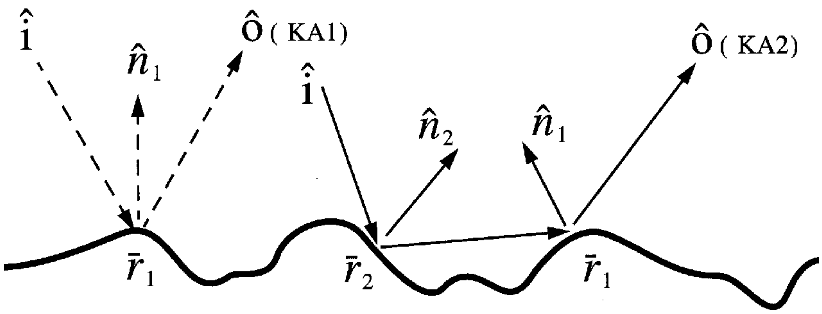

Figure 3. First-and second-order Kirchhoff approximations. The dotted lines are for the first-order, and the solid lines are for the second-order Kirchhoff approximations. $\hat{n}_1$ and $\hat{n}_2$ are chosen to be at the staionary phase points.

Let us now consider the far-field scattering; we approximate g in (1) by

$$g = \frac{\exp[ikR - i\overline{K} \cdot \overline{r}_1]}{4\pi R}, \ \overline{K} = k\hat{o} \tag{3}$$

where R is the range from the surface to the receiver. Also note that $\nabla = i\overline{K}$, and thus we can write (1) as

$$\overline{E} = \frac{e^{ikR}}{R}\overline{F} \tag{4}$$

where

$$\overline{F} = (i\overline{K}) \times (i\overline{K}) \times \frac{i}{4\pi\omega\epsilon_0} \int \hat{n}_1 \times \overline{H}_{1s} e^{-i\overline{K}\cdot\overline{r}_1} dS_1$$
$$- \frac{(i\overline{K})}{4\pi} \times \int \overline{E}_{1s} \times \hat{n}_1 e^{-i\overline{K}\cdot\overline{r}_1} dS_1$$

If we rewrite this as

$$\begin{bmatrix} E_\theta \\ E_\phi \end{bmatrix} = \frac{e^{ikR}}{R} \begin{bmatrix} f_{11} & f_{12} \\ f_{21} & f_{22} \end{bmatrix} \begin{bmatrix} E_{i\theta} \\ E_{i\phi} \end{bmatrix} \tag{5}$$

then we can express the 4x4 Mueller matrix $[M]$ relating the scattered specific intensity $[I_s]$ to the incident specific intensity $[I_i]$.

$$[I_s] = \frac{1}{R^2}[M][I_i] \tag{6}$$

where

$$[I_s] = \begin{bmatrix} \langle |E_\theta|^2 \rangle \\ \langle |E_\phi|^2 \rangle \\ 2Re\langle E_\theta E_\phi^* \rangle \\ 2Im\langle E_\theta E_\phi^* \end{bmatrix}, [I_i] = \begin{bmatrix} \langle |E_{i\theta}|^2 \rangle \\ \langle |E_{i\phi}|^2 \rangle \\ 2Re\langle E_{i\theta} E_{i\phi}^* \rangle \\ 2Im\langle E_{i\theta} E_{i\phi}^* \rangle \end{bmatrix}$$

$$[M] = \begin{bmatrix} \langle |f_{11}|^2 \rangle & \langle |f_{12}|^2 \rangle & \mathrm{Re}\langle f_{11} f_{12}^* \rangle & -\mathrm{Im}\langle f_{11} f_{12}^* \rangle \\ \langle |f_{21}|^2 \rangle & \langle |f_{22}|^2 \rangle & \mathrm{Re}\langle f_{21} f_{22}^* \rangle & -\mathrm{Im}\langle f_{21} f_{22}^* \rangle \\ 2\mathrm{Re}\langle f_{11} f_{21}^* \rangle & 2\mathrm{Re}\langle f_{12} f_{22}^* \rangle & \mathrm{Re}\langle f_{11} f_{22}^* + f_{12} f_{21}^* \rangle & -\mathrm{Im}\langle f_{11} f_{22}^* - f_{12} f_{21}^* \rangle \\ 2\mathrm{Im}\langle f_{11} f_{21}^* \rangle & 2\mathrm{Im}\langle f_{12} f_{22}^* \rangle & \mathrm{Im}\langle f_{11} f_{22}^* + f_{12} f_{21}^* \rangle & \mathrm{Re}\langle f_{11} f_{22}^* - f_{12} f_{21}^* \rangle \end{bmatrix}$$

The corresponding 4×4 cross section Mueller matrix per unit area is then given by

$$[\sigma] = \frac{4\pi}{A}[M] \tag{7}$$

where A is the illuminated surface area.

3. First-Order Kirchhoff and Geometric Optics Approximation

The first-order Kirchhoff approximation has been studied extensively in the past. Here we give a brief summary using matrix notation which will be useful for the second-order Kirchhoff approximation to be described in the following section.

The incident wave is given by $\overline{E}_i = \overline{e}_i \exp\,[i\overline{K}_i \cdot \overline{r}_1]$ and $\overline{H}_i = \overline{h}_i \exp\,[i\overline{K}_i \cdot \overline{r}_1]$ with $\overline{K}_i = k\hat{\imath}$. Thus writing the scattered wave as $\overline{E}_{1s} = \overline{e}_{1s} \exp\,[i\overline{K}_i \cdot \overline{r}_1]$ and $\overline{H}_{1s} = \overline{h}_{1s} \exp\,[i\overline{K}_i \cdot \overline{r}_1]$, we get

$$\overline{E}_{KA1} = \frac{e^{ikR}}{R}\overline{F}_1 \tag{8}$$

$$\begin{aligned}\overline{F}_1 = (i\overline{K}) \times (i\overline{K}) \times \frac{i}{4\pi\omega\epsilon_0}\int \hat{n}_1 \times \overline{h}_{1s} e^{-i(\overline{K}-\overline{K}_i)\cdot\overline{r}_1} dS_1 \\ - (i\overline{K}) \times \frac{1}{4\pi}\int \overline{e}_{1s} \times \hat{n}_1 e^{-i(\overline{K}-\overline{K}_i)\cdot\overline{r}_1} dS_1\end{aligned}$$

Since this is the Kirchhoff approximation, $\overline{e}_{1s}$ and $\overline{h}_{1s}$ are zero in shadow regions and will be taken care of by the shadowing function later.

Let us first examine $\overline{e}_{1s}$. This is the field locally reflected by the surface, and the reflection coefficients are different depending on the polarization. The reflection coefficient for the polarization (p-pol) parallel to the plane of incidence is given by (Figure 4)

$$R_{\|} = \frac{\sqrt{\epsilon_0}\cos\theta_1 - \sqrt{\epsilon_1}\cos\theta_0}{\sqrt{\epsilon_0}\cos\theta_1 + \sqrt{\epsilon_1}\cos\theta_0} \tag{9}$$

For perpendicular polarization (s-pol), we have

$$R_{\perp} = \frac{\sqrt{\epsilon_0}\cos\theta_0 - \sqrt{\epsilon_1}\cos\theta_1}{\sqrt{\epsilon_0}\cos\theta_0 + \sqrt{\epsilon_1}\cos\theta_1} \tag{10}$$

where $\cos\theta_0 = \hat{\imath}\cdot\hat{n}_1$ and $\sqrt{\epsilon_0}\sin\theta_0 = \sqrt{\epsilon_1}\sin\theta_1$. Using the unit vectors $\hat{p}$ and $\hat{q}$ in the directions parallel to and perpendicular to the plane of incidence, respectively, and using $\hat{p}_r$ for the reflected wave for parallel polarization, we write (Figure 4).

$$\overline{e}_{1s} = R_{\|}\hat{p}_r(\hat{p}\cdot\overline{e}_i) + R_{\perp}\hat{q}(\hat{q}\cdot\overline{e}_i) \tag{11}$$

where

$$\begin{aligned}\hat{q} = \frac{\hat{\imath} \times \hat{n}_1}{|\hat{\imath} \times \hat{n}_1|}, \quad \hat{p} = \hat{q} \times \hat{\imath}, \\ \hat{p}_r = -\hat{q} \times \hat{r}, \quad \hat{r} = \hat{\imath} - 2\hat{n}_1(\hat{n}_1 \cdot \hat{\imath})\end{aligned}$$

For the magnetic field $\overline{h}_{1s}$, we get

$$\overline{h}_{1s} = \sqrt{\frac{\epsilon_0}{\mu_0}}\hat{r} \times \overline{e}_{1s} \tag{12}$$

We also note that under the geometric optics approximation, $\hat{n}_1$ is constant and equal to its value at the stationary phase point.

$$\hat{n}_1 = \frac{\overline{K} - \overline{K}_i}{|\overline{K} - \overline{K}_i|} \tag{13}$$

Thus equation (8) is given by

$$\begin{aligned} \overline{F}_1 = \frac{i}{4\pi}\left(-(\overline{K} \times \overline{K} \times \hat{n}_1 \times \hat{r} \times \overline{e}_{1s})\frac{1}{k} + (\overline{K} \times \hat{n}_1 \times \overline{e}_{1s})\right) \\ \times \int e^{-i(\overline{K}-\overline{K}_i)\cdot\overline{r}_1} dS_1 \end{aligned} \tag{14}$$

where it is understood that the surface integral is over the illuminated area.

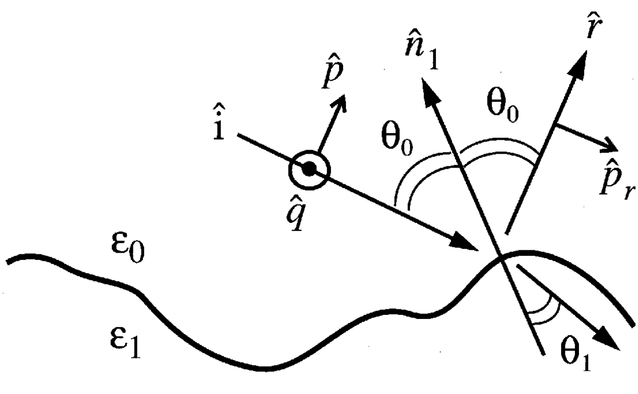

Figure 4. Reflection coefficients.

The cross product in (14) can be expressed using the antisymmetric matrix in the Cartesian coordinate system. For example $\overline{B} \times \overline{C}$ is expressed by

$$[\overline{\overline{B}}][C] = \begin{bmatrix} 0 & -B_z & B_y \\ B_z & 0 & -B_x \\ -B_y & B_x & 0 \end{bmatrix} \begin{bmatrix} C_x \\ C_y \\ C_z \end{bmatrix} \tag{15}$$

Also we can express $\overline{A} \times (\overline{B} \times \overline{C})$ by $\left[\overline{\overline{A}}\right] \left[\overline{\overline{B}}\right] [C]$ where $\left[\overline{\overline{A}}\right]$ is the antisymmetric matrix as shown in (15). Note that $\overline{A} \times (\overline{B} \times \overline{C})$ is not associative; $\overline{A} \times (\overline{B} \times \overline{C}) \neq (\overline{A} \times \overline{B}) \times \overline{C}$. However with the antisymmetric tensor matrix, the product is associative,

$$\left[\overline{\overline{A}}\right] \left(\left[\overline{\overline{B}}\right] [C] \right) = \left(\left[\overline{\overline{A}}\right] \left[\overline{\overline{B}}\right] \right) [C]$$

Using the antisymmetric matrix, we can express (14) in a more compact matrix form. We get

$$\begin{aligned} f_{11} &= [\theta]^\dagger [H][\theta_i] J_1 = H_{11} J_1 \\ f_{12} &= [\theta]^\dagger [H][\phi_i] J_1 = H_{12} J_1 \\ f_{21} &= [\phi]^\dagger [H][\theta_i] J_1 = H_{21} J_1 \\ f_{22} &= [\phi]^\dagger [H][\phi_i] J_1 = H_{22} J_1 \end{aligned} \tag{16}$$

where $[\theta]^\dagger$ is the transpose of $[\theta]$, $[\phi]^\dagger$ is the transpose of $[\phi]$, and

$$[H] = \frac{1}{4\pi} \left(-i \left[\overline{\overline{K}}\right] \left[\overline{\overline{K}}\right] [\overline{\overline{n_1}}] [\overline{\overline{r}}] \frac{1}{k} + \left[\overline{\overline{K}}\right] [\overline{\overline{n_1}}] \right) [e_{1s}] \tag{17}$$

$$[e_{1s}] = R_{||} [p_r][p]^\dagger + R_\perp [q][q]^\dagger$$

Also note that

$$\begin{aligned} [q] &= \frac{[\overline{\overline{i}}][n_1]}{\sqrt{1 - \left([i]^\dagger [n_1] \right)^2}} \\ [p] &= [\overline{\overline{q}}][i] \\ [p_r] &= [\overline{\overline{r}}][q] \\ [r] &= [i] - 2[n_1] \left([n_1]^\dagger [i] \right) \\ J_1 &= \int e^{-i(\overline{K} - \overline{K}_i) \cdot \overline{r}_1} dS_1 \\ [n_1] &= \frac{[o] - [i]}{\sqrt{([o] - [i])^\dagger ([o] - [i])}} \end{aligned} \tag{18}$$

If the incident wave is in the $x - z$ plane, we have, in Cartesian system,

$$[\theta] = \begin{bmatrix} \cos\theta \cos\phi \\ \cos\theta \sin\phi \\ -\sin\theta \end{bmatrix}, [\theta_i] = \begin{bmatrix} -\cos\theta_i \\ 0 \\ -\sin\theta_i \end{bmatrix},$$

$$[\phi] = \begin{bmatrix} -\sin\phi \\ \cos\phi \\ 0 \end{bmatrix}, \qquad [\phi_i] = \begin{bmatrix} 0 \\ 1 \\ 0 \end{bmatrix},$$

$$[K] = k[o], \qquad [K_i] = k[i],$$

$$[o] = \begin{bmatrix} \sin\theta\cos\phi, \\ \sin\theta\sin\phi \\ \cos\theta \end{bmatrix}, [i] = \begin{bmatrix} \sin\theta_i \\ 0 \\ -\cos\theta_i \end{bmatrix}.$$

The cross sections per unit area of the rough surface are then given by

$$\begin{aligned} \sigma_{\theta\theta} &= \sigma_{vv} = \frac{4\pi}{A}|H_{11}|^2 I^{(1)} \\ \sigma_{\theta\phi} &= \sigma_{vh} = \frac{4\pi}{A}|H_{12}|^2 I^{(1)} \\ \sigma_{\phi\theta} &= \sigma_{hv} = \frac{4\pi}{A}|H_{21}|^2 I^{(1)} \\ \sigma_{\phi\phi} &= \sigma_{hh} = \frac{4\pi}{A}|H_{22}|^2 I^{(1)} \end{aligned} \tag{19}$$

where

$$I^{(1)} = (\langle J_1 J_1^* \rangle - \langle J_1 \rangle \langle J_1^* \rangle)$$

Note that the coherent component $\langle J_1 \rangle$ is negligibly small for very rough surfaces. The complete cross section Mueller matrix is obtained using (16) in (6) and (7).

4. Evaluation of $\langle J_1 J_1^* \rangle$ in the Geometric Optics Approximation

In the geometric optics approximation, $\langle J_1 \rangle$ is negligibly small. $\langle J_1 \rangle$ is given by

$$\langle J_1 \rangle = \int \langle e^{-i(\overline{K}-\overline{K}_i)\cdot\overline{r}} \rangle dS_1 \tag{20}$$

Letting

$$\overline{r} = \overline{x} + f(x, y)\hat{z} \quad on\, the\, surface,$$

$$dS_1 = \frac{d\overline{x}}{N_z}, d\overline{x} = dxdy,$$

$$\begin{aligned} N_z = \hat{n}_1 \cdot \hat{z} = \frac{K_z - K_{iz}}{|K - K_i|} \\ = \frac{\cos\theta + \cos\theta_i}{\sqrt{2\left(1 + \cos\theta\cos\theta_i - \sin\theta\cos\phi\sin\theta_i\right)}} \end{aligned}$$

$$\overline{K} - \overline{K}_i = \overline{v} + v_z\hat{z},$$

$$\begin{aligned} \overline{K} &= \overline{\kappa} + K_z\hat{z}, & \overline{K}_i &= \overline{\kappa}_i + K_{iz}\hat{z}, \\ \overline{v} &= \overline{\kappa} - \overline{\kappa}_i, & v_z &= K_z - K_{iz} \end{aligned}$$

we get

$$\langle J_1 \rangle = \int e^{-i\overline{v}\cdot\overline{x}} \left\langle e^{-iv_z f} \right\rangle \frac{d\overline{x}}{N_z} \tag{21}$$

This integral is over the illuminated region and therefore can be expressed by the following integral over the entire surface using the shadowing correction S_c.

$$\langle J_1 \rangle = \int e^{-i\overline{v}\cdot\overline{x}} \langle e^{-iv_z f} \rangle \frac{d\overline{x}}{N_z} S_c \tag{22}$$

The shadowing correction S_c represents the probability that the surface is illuminated by the incident wave. If f is a Gaussian random variable, then

$$\langle e^{-ivf} \rangle = e^{-\frac{1}{2}v^2\sigma^2}, \sigma^2 = \langle f^2 \rangle \tag{23}$$

Also note

$$\int e^{-i(\overline{\kappa}-\overline{\kappa}_i)\cdot\overline{x}} d\overline{x} = (2\pi)^2 \delta(\overline{\kappa} - \overline{\kappa_i}) \tag{24}$$

Thus we get

$$\langle J_1 \rangle = (2\pi)^2 \delta(\overline{\kappa} - \overline{\kappa_i}) \frac{e^{-2k^2\sigma^2\cos^2\theta_i}}{N_z} S_c \tag{25}$$

where $S_c^2 = S(\theta_i, \theta_i)$, and $S(\theta_i, \theta)$ is the shadowing function to be described later. It is clear that $\langle J_1 \rangle$ is negligibly small for large $k\sigma\cos\theta_i$.

Now consider $I^{(1)} = \langle J_1 J_1^* \rangle$; we get

$$I^{(1)} = \int\int \frac{d\overline{x}_1 d\overline{x}'_1}{{N_z}^2} e^{-i\overline{v}\cdot\overline{x}_d} \langle e^{-iv_z f_1 + iv_z f_1{}'} \rangle \tag{26}$$

where $\overline{v} = \overline{\kappa} - \overline{\kappa}_i$, $\overline{x}_d = \overline{x}_1 - \overline{x}'_1$, $f_1 = f(\overline{x}_1)$, $f_1{}' = f(\overline{x}'_1)$, and $v_z = K_z - K_{iz}$. Now, for Gaussian variables f_1 and f_2 , we have

$$\langle \exp\ -iv_1 f_1 - iv_2 f_2 \rangle = \exp\ -\frac{1}{2}\left({v_1}^2{\sigma_1}^2 + 2v_1 v_2 \sigma_1 \sigma_2 C + {v_2}^2{\sigma_2}^2\right) \tag{27}$$

where ${\sigma_1}^2 = \langle {f_1}^2 \rangle$, ${\sigma_2}^2 = \langle {f_2}^2 \rangle$, $C = \langle f_1 f_2 \rangle / (\sigma_1 \sigma_2)$, and $v_1 = -v_2 = v_z$. For very rough surfaces, ${v_z}^2\sigma^2 \gg 1$, and therefore we expand C in a series of powers of $|\overline{x}_1 - \overline{x}'_1|$ and keep the first two terms,

$$C \cong 1 - \frac{|\overline{x}_1 - \overline{x}'_1|^2}{l^2} \tag{28}$$

where l is the correlation distance. Thus we get

$$\langle e^{-iv_z f_1 + iv_z f_2} \rangle = \exp\left[-{v_z}^2\sigma^2 \frac{{x_d}^2}{l^2}\right] \tag{29}$$

where ${x_d}^2 = |\overline{x}_1 - \overline{x}'_1|^2$. Substituting this into (26), we get

$$I^{(1)} = \frac{A}{{N_z}^2} \frac{\pi l^2}{{v_z}^2\sigma^2} \exp\left[-\frac{v^2 l^2}{4{v_z}^2\sigma^2}\right] S \tag{30}$$

where

$${v_z}^2 = k^2 (\cos\theta + \cos\theta_i)^2$$

$$v = |\overline{\kappa} - \overline{\kappa}_i| = k\sqrt{\sin^2\theta + \sin^2\theta_i - 2\sin\theta\sin\theta_i\cos\phi}$$

The shadowing function by Wagner is given by the following [25]: In the back direction, $\phi = \pi$ and $\phi_i = 0$,

$$S = S(\theta_1) \qquad for \quad 0 < \theta < \theta_i \tag{31}$$

$$S = S(\theta_2) \qquad for \quad \theta_i < \theta < \frac{\pi}{2} \tag{32}$$

In all other directions, S is approximately given by

$$S = S(\theta_1, \theta_2) \tag{33}$$

The functions $S(\theta_1)$, $S(\theta_2)$ and $S(\theta_1, \theta_2)$ are given by

$$S(\theta_k) = (1 + erf\,[v_k])\left(1 - \epsilon^{-F_k}\right)\frac{1}{2F_k} \tag{34}$$

$$S(\theta_1, \theta_2) = \left(1 - \epsilon^{-(F_1+F_2)}\right)\frac{erf\,[v_1] + erf\,[v_2]}{2\,(F_1 + F_2)} \tag{35}$$

where

$$\theta_1 = \frac{\pi}{2} - \theta_i, \qquad \theta_2 = \frac{\pi}{2} - \theta,$$

$$v_k = \frac{|\tan\theta_k|}{2\sigma\,/\,l}, \qquad k = 1, 2,$$

$$F_k = \frac{1}{2}\left(\frac{e^{-9{v_k}^2\,/\,8}}{\sqrt{3\pi}v_k} + \frac{e^{-v_k^2}}{\sqrt{\pi}v_k} - (1 - erf\,[v_k])\right)$$

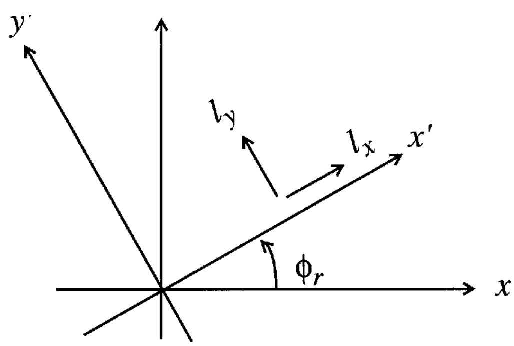

Figure 5. Anisotropic rough surface with the correlation distance l_x in the x' direction and l_y in the y' direction.

If the rough surface is anisotropic such that the correlation distance is l_x in the x' direction and l_y in the y' direction (Figure 5), then $I^{(1)}$ in (30) should be modified to the following:

$$I^{(1)} = \frac{A}{{N_z}^2}\frac{\pi l_x l_y}{{v_z}^2\sigma^2}\,\exp\left[-\frac{\left[(\overline{\kappa} - \overline{\kappa}_i)\cdot\hat{x}'\right]^2 {l_x}^2}{4{v_z}^2\sigma^2} - \frac{\left[(\overline{\kappa} - \overline{\kappa}_i)\cdot\hat{y}'\right]^2 {l_y}^2}{4{v_z}^2\sigma^2}\right] S \tag{36}$$

For the shadowing function in (36), the correlation distance l should be modified to

$$l^2 = \left(l_x \left(\frac{\overline{v} \cdot \hat{x}'}{v}\right)\right)^2 + \left(l_y \left(\frac{\overline{v} \cdot \hat{y}'}{v}\right)\right)^2 \tag{37}$$

5. Second-Order Kirchhoff Approximation

The field at $\overline{r}_1$ consists of the first- and second-order Kirchhoff approximations, and we have already discussed the first-order case. The second-order Kirchhoff field at $\overline{r}_1$ is obtained using the first-order Kirchhoff approximation at $\overline{r}_2$ and propagation from $\overline{r}_2$ to $\overline{r}_1$.

The field $\overline{E}_1(\overline{r}_1)$ at $\overline{r}_1$ due to second-order Kirchhoff is given by

$$\overline{E}_1(\overline{r}_1) = \nabla \times \nabla \times \overline{\pi} + i\omega\mu\nabla \times \bar{\pi}_m \tag{38}$$

$$\begin{aligned} \overline{\pi} &= \frac{i}{\omega\epsilon_0} \int \hat{n}_2 \times \overline{H}_2 g_2 \, dS_2 \\ \overline{\pi}_m &= \frac{i}{\omega\mu} \int \overline{E}_2 \times \hat{n}_2 g_2 dS_2 \end{aligned} \tag{39}$$

where

$$g_2 = \frac{\epsilon^{ik|\overline{r}_1 - \overline{r}_2|}}{4\pi|\overline{r}_1 - \overline{r}_2|}.$$

$\overline{E}_2$ and $\overline{H}_2$ are the fields at $\overline{r}_2$ which are found using the Kirchhoff approximation. We also use real rays from $\overline{r}_2$ to $\overline{r}_1$, neglecting evanescent waves, which is consistent with the geometric optics approximation. Green's function g_2 is now expressed in Weyl's integral in the y-z plane.

$$g_2 = \frac{ik}{8\pi^2} \int_0^{2\pi} d\beta \int_C \sin\alpha \, d\alpha \, e^f \tag{40}$$

$$\begin{aligned} f = {} & i\,(k \sin\alpha \cos\beta)\,(y_1 - y_2) \\ & + i\,(k \sin\alpha \sin\beta)\,(z_1 - z_2) \\ & + i\,(k \cos\alpha)\,|x_1 - x_2| \end{aligned}$$

where C is the contour from $\alpha = 0$ to $\pi/2$ to $-i\infty$. However, to be consistent with the geometric optics approximation, we use only the real ray from $\alpha = 0$ to $\pi/2$ and ignore the evanescent wave. For convenience we use the angles α_0 and ψ_0 in Figure 6 and get

$$g_2(\overline{r}_1 - \overline{r}_2) = \frac{ik}{8\pi^2} \int_{-\pi/2}^{\pi/2} d\psi_0 \int_{-\pi/2}^{\pi/2} \cos\alpha_0 d\alpha_0 e^{i\overline{K}_1 \cdot (\overline{r}_1 - \overline{r}_2)} \tag{41}$$

where

$$\overline{K}_1 = \overline{K}_{1+} = k\cos\alpha_0 \cos\psi_0\, \hat{x} + k\cos\alpha_0 \sin\psi_0\, \hat{y} + k\sin\alpha_0\, \hat{z} \quad \text{for } x_1 > x_2$$

$$\overline{K}_1 = \overline{K}_{1-} = -\overline{K}_{1+} \qquad \text{for } x_1 < x_2$$

Note that $\overline{K}_{1-}$ is obtained from $\overline{K}_{1+}$ by changing $\alpha_0 \to -\alpha_0$ and $\psi_0 \to \psi_0 + \pi$.

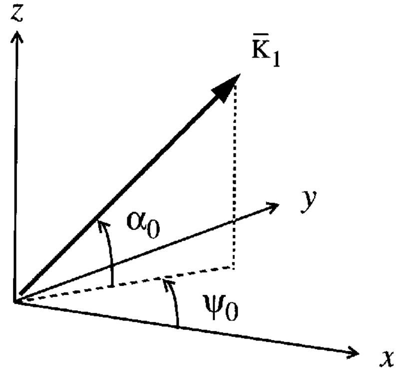

Figure 6. The wave number vector $\overline{K_1}$ in real space for the Green's function g_2

The field $\overline{E}_1$ at $\overline{r}_1$ can be expressed using the 3x3 matrix $[H]$ in (17). The matrix $[H]$ is a function of $\overline{K}$ and $\bar{K}_i$ for the first-order Kirchhoff approximation. For second-order scattering, we use $[H]_2$ which is a function of $\overline{K}_1$ and $\overline{K}_i$ to represent the Kirchhoff approximation at $\overline{r}_2$ and propagation from $\overline{r}_2$ to $\overline{r}_1$, and $[H]_1$ which is a function of $\overline{K}$ and $\overline{K}_1$ to represent the scattering at $\overline{r}_1$ in the direction of $\overline{K}$. Thus, we get

$$\begin{aligned} [F_{KA2}] &= \mathcal{L}[H]^{(2)} J_2 \\ [H]^{(2)} &= [H]_1 [H]_2 \end{aligned} \tag{42}$$

where

$$\mathcal{L} = \frac{ik}{2\pi} \int_{-\pi/2}^{\pi/2} d\psi_0 \int_{-\pi/2}^{\pi/2} \cos\alpha_0 \, d\alpha_0$$

$$[H]_1 = [H] \text{ with } \overline{K} \text{ and } \overline{K}_1$$

$$[H]_2 = [H] \text{ with } \overline{K}_1 \text{ and } \overline{K}_i$$

$$J_2 = \int\int e^{-i(\overline{K}-\overline{K}_1)\cdot\overline{r}_1 - i(\overline{K}_1-\overline{K}_i)\cdot\overline{r}_2} \, dS_1 \, dS_2$$

where the surface integrals are over the illuminated region, which will be represented by shadowing corrections later.

The cross section Mueller matrix per unit area of the rough surface for the second-order Kirchhoff approximation is then given by

$$\begin{aligned}
\sigma_{\theta\theta} = \sigma_{vv} &= \frac{4\pi}{A} \mathcal{L}\mathcal{L}'^* H_{11}^{(2)} H_{11}^{(2)\prime *} I^{(2)} \\
\sigma_{\theta\phi} = \sigma_{vh} &= \frac{4\pi}{A} \mathcal{L}\mathcal{L}'^* H_{12}^{(2)} H_{12}^{(2)\prime *} I^{(2)} \\
\sigma_{\phi\theta} = \sigma_{hv} &= \frac{4\pi}{A} \mathcal{L}\mathcal{L}'^* H_{21}^{(2)} H_{21}^{(2)\prime *} I^{(2)} \\
\sigma_{\phi\phi} = \sigma_{hh} &= \frac{4\pi}{A} \mathcal{L}\mathcal{L}'^* H_{22}^{(2)} H_{22}^{(2)\prime *} I^{(2)}
\end{aligned} \tag{43}$$

where

$$I^{(2)} = \langle J_2 {J_2}^* \rangle - \langle J_2 \rangle \langle {J_2}^* \rangle$$

$$\begin{aligned}
H_{11}^{(2)} &= [\theta]^\dagger [H]^{(2)} [\theta_i] \\
H_{12}^{(2)} &= [\theta]^\dagger [H]^{(2)} [\phi_i] \\
H_{21}^{(2)} &= [\phi]^\dagger [H]^{(2)} [\theta_i] \\
H_{22}^{(2)} &= [\phi]^\dagger [H]^{(2)} [\phi_i]
\end{aligned} \tag{44}$$

6. Evaluation of the Ladder Term $\langle J_{2+} {J_{2+}}^* \rangle$

The expression for J_2 is given in (42). However, as stated in (41), J_2 consists of the term J_{2+} for $x_1 > x_2$ and the term J_{2-} for $x_1 < x_2$.

$$J_2 = J_{2+} + J_{2-} \tag{45}$$

We can therefore write

$$\langle J_2 J_2{}^* \rangle = \langle J_{2+} J_{2+}{}^* \rangle + \langle J_{2-} J_{2-}{}^* \rangle + 2Re \langle J_{2+} J_{2-}{}^* \rangle \tag{46}$$

The first two terms of (46) represent the ladder term, and the last one represents the cross term which gives rise to enhanced backscattering.

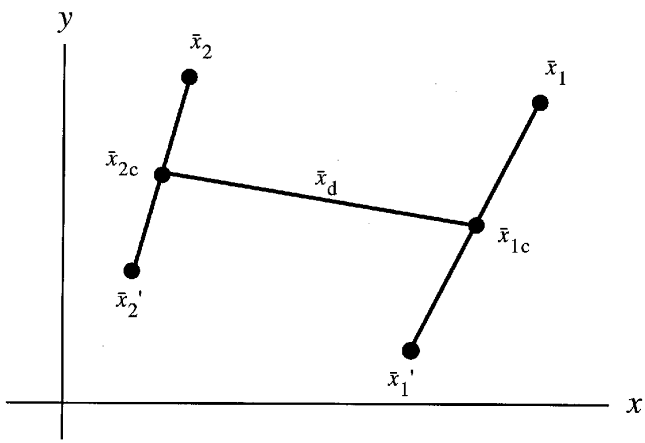

Figure 7. Change of variables.

Let us first consider $\langle J_{2+} J_{2+}{}^* \rangle$. Here we use $\overline{K_1} = \overline{K}_{1+}$. On the surface, $\overline{r}_1 = \overline{x}_1 + f_1 \hat{z}$ and $\overline{r}_2 = \overline{x}_2 + f_2 \hat{z}$. We also use

$$\begin{aligned} \overline{K} &= \overline{\kappa} + K_z \hat{z} \\ \overline{K}_1 &= \overline{\kappa}_1 + K_{1z} \hat{z} \\ \overline{K}_i &= \overline{\kappa}_i + K_{iz} \hat{z} \end{aligned} \tag{47}$$

$$dS_1 = \frac{d\overline{x}_1}{N_{z1}}, \quad dS_2 = \frac{d\overline{x}_2}{N_{z2}}$$

$$\begin{aligned} N_{z1}^2 &= \frac{(\cos\theta - \sin\alpha_0)^2}{2\,(1 - \sin\theta\cos\alpha_0\cos(\phi - \psi_0) - \cos\theta\sin\alpha_0)} \\ N_{z2}^2 &= \frac{(\sin\alpha_0 + \cos\theta_i)^2}{2\,(1 - (\cos\alpha_0\sin\theta_i\cos\psi_0 + \sin\alpha_0\cos\theta_i))} \end{aligned}$$

We also use the following change of variables from $\overline{x}_1$, $\overline{x}_1'$, $\overline{x}_2$, $\overline{x}_2'$ to $\overline{x}_{1d}$, $\overline{x}_{1c}$, $\overline{x}_{2d}$, $\overline{x}_{2c}$, see Figure 7.

$$\begin{aligned}\overline{x}_{1d} &= \overline{x}_1 - \overline{x}_1' \\ \overline{x}_{1c} &= \left(\overline{x}_1 + \overline{x}_1'\right) / 2 \\ \overline{x}_{2d} &= \overline{x}_2 - \overline{x}_2' \\ \overline{x}_{2c} &= \left(\overline{x}_2 + \overline{x}_2'\right) / 2\end{aligned} \tag{48}$$

Furthermore, we use

$$\begin{aligned}\overline{x}_d &= \overline{x}_{1c} - \overline{x}_{2c} \\ \overline{x}_c &= \left(\overline{x}_{1c} + \overline{x}_{2c}\right) / 2\end{aligned} \tag{49}$$

Also note that

$$e^{-i\overline{a}\cdot\overline{x}_1 + i\overline{b}\cdot\overline{x}_2} = e^{-i\overline{c}\cdot\overline{x}_d - i\overline{d}\cdot\overline{x}_c} \tag{50}$$

where

$$\begin{aligned}\overline{c} &= \left(\overline{a} + \overline{b}\right) / 2, \qquad & \overline{d} &= \overline{a} - \overline{b}, \\ \overline{x}_c &= \left(\overline{x}_1 + \overline{x}_2\right) / 2, \qquad & \overline{x}_d &= \overline{x}_1 - \overline{x}_2\end{aligned}$$

It is also reasonable to use the approximation that f_1 and f_2 are uncorrelated. Thus, we get

$$\langle J_{2+} J_{2+}{}^{*} \rangle = \frac{A}{\left(N_{z1} N_{z2}\right)\left(N_{z1}{}' N_{z2}{}'\right)} \, \phi_1 \, \phi_2 \, F_d \, S_2 \tag{51}$$

where

$$\begin{aligned}\phi_1 &= \int e^{-i\overline{c}_1\cdot\overline{x}_{1d}} B_1(x_{1d}) d\overline{x}_{1d} \\ \phi_2 &= \int e^{-i\overline{c}_2\cdot\overline{x}_{2d}} B_2(x_{2d}) d\overline{x}_{2d} \\ \overline{v}_{1c} &= \left(\left(\overline{\kappa} - \overline{\kappa}_1\right) + \left(\overline{\kappa} - \overline{\kappa}_1'\right)\right) / 2 = \left(\overline{v}_1 + \overline{v}_1'\right) / 2 \\ \overline{v}_{2c} &= \left(\left(\overline{\kappa}_1 - \overline{\kappa}_i\right) + \left(\overline{\kappa}_1' - \overline{\kappa}_i\right)\right) / 2 = \left(\overline{v}_2 + \overline{v}_2'\right) / 2 \\ B_1(x_{1d}) &= \langle e^{-i(K_z - K_{1z}) f_1 + i(K_z - K_{1z}{}') f_1{}'} \rangle \\ &= \langle e^{-i v_{1z} f_1 + i v_{1z}{}' f_1{}'} \rangle \\ B_2(x_{2d}) &= \langle e^{-i(K_{1z} - K_{iz}) f_2 + i(K_{1z}{}' - K_{iz}{}') f_2{}'} \rangle \\ &= \langle e^{-i v_{2z} f_2 + i v_{2z}{}' f_2{}'} \rangle\end{aligned}$$

where

$$\begin{aligned}
\overline{v}_1 &= \overline{\kappa} - \overline{\kappa}_1, \quad \overline{v}'_1 = \overline{\kappa} - \overline{\kappa}'_1 \\
\overline{v}_2 &= \overline{\kappa}_1 - \overline{\kappa}_i, \quad \overline{v}'_2 = \overline{\kappa}'_1 - \overline{\kappa}_i \\
\overline{\kappa} &= k\sin\theta\cos\phi\,\hat{x} + k\sin\theta\sin\phi\,\hat{y} \\
\overline{\kappa}_i &= k\sin\theta_i\,\hat{x} \\
\overline{\kappa}_1 &= k\cos\alpha_0\cos\psi_0\,\hat{x} + k\cos\alpha_0\sin\psi_0\,\hat{y} \\
\overline{\kappa}'_1 &= k\cos{\alpha_0}'\cos{\psi_0}'\,\hat{x} + k\cos{\alpha_0}'\sin{\psi_0}'\,\hat{y} \\
v_{1z} &= K_z - K_{1z} = k\cos\theta - k\sin\alpha_0 \\
{v_{1z}}' &= K_z - {K_{1z}}' = k\cos\theta - k\sin{\alpha_0}' \\
v_{2z} &= K_{1z} - K_{iz} = k\sin\alpha_0 + k\cos\theta_i \\
{v_{2z}}' &= {K_{1z}}' - K_{iz} = k\sin{\alpha_0}' + k\cos\theta_i \\
\overline{v}_{1c} &= \left(\overline{v}_1 + \overline{v}'_1\right)\,/\,2 \\
\overline{v}_{2c} &= \left(\overline{v}_2 + \overline{v}'_2\right)\,/\,2
\end{aligned}$$

F_d represents the propagation from $\overline{r}_2$ to $\overline{r}_1$.

$$F_d = \int e^{-i(\overline{K}'_1 - \overline{K}_1)\cdot\overline{x}_d}\, S_p(x_d)\, d\overline{x}_d \tag{52}$$

$S_p(x_d)$ is the propagation shadowing function, and S_2 is the angular shadowing function for the second-order Kirchhoff approximation.

Let us first consider B_1 . We assume that the height f_1 is normally distributed, and therefore we use

$$\left\langle e^{-iv_1 f_1 - iv_2 f_2}\right\rangle = e^{-\frac{1}{2}\left(v_1^2\sigma_1^2 + v_2^2\sigma_2^2 + 2v_1v_2\sigma_1\sigma_2 C\right)} \tag{53}$$

where $\sigma_1^2 = \langle f_1^2\rangle$, $\sigma_2^2 = \langle f_2^2\rangle$ and $C = \langle f_1 f_2\rangle\,/\,(\sigma_1\sigma_2)$. For our problem in (51), we get

$$B_1(x_{1d}) = \exp\left[-\frac{\sigma^2}{2}\left(v_{1z}^2 + {v_{1z}}'^2 - 2\,v_{1z}{v_{1z}}'\,C(x_{1d})\right)\right] \tag{54}$$

We also use the geometric optics approximation, (28), and obtain

$$\phi_1 = e^{-\frac{\sigma^2}{2}(v_{1z} - {v_{1z}}')^2}\left(\frac{\pi l^2}{\sigma^2 v_{1z}{v_{1z}}'}\right)\exp\left[-\frac{v_{1c}^2 l^2}{4\sigma^2 v_{1z}{v_{1z}}'}\right] \tag{55}$$

where $v_{1c} = |\overline{v}_{1c}| = (\overline{v}_1 + \overline{v}_1')\,/\,2$. Similarly, we get

$$\phi_2 = e^{-\frac{\sigma^2}{2}(v_{2z} - v_{2z}')^2} \left(\frac{\pi l^2}{\sigma^2 v_{2z} v_{2z}'} \right) \exp\left[-\frac{v_{2c}^2 l^2}{4\sigma^2 v_{2z} v_{2z}'} \right] \tag{56}$$

where $v_{2c} = |\overline{v}_{2c}|, \quad \overline{v}_{2c} = (\overline{v}_2 + \overline{v}_2')\,/\,2$

Now consider the propagation shadowing function $S_p(x_d)$. As shown in [17] and [18], we note that the second-order wave propagates only over the distance until it is intersected by the surface. Thus we write $S_p(x_d)$ as

$$S_p(x_d) = e^{-x_d^2\,/\,D^2} \tag{57a}$$

belive where D is the mean distance the wave propagates without being interrupted by the surface. For D, we use the mean duration of a fade at the level $h_0 = \sqrt{2}\sigma$ given by

$$D(h_0) = \frac{\pi}{\Omega} e^{h_0^2\,/\,(2\sigma^2)} \left(1 + \operatorname{erf}\left[\frac{h_0}{\sqrt{2}\sigma} \right] \right) \tag{57b}$$

where $\Omega = \sqrt{2}\,/\,l$. We then get $D = 11.13l$ [17]. The integral for F_d in (51) can now be evaluated for $x_1 > x_2$. We have

$$\int d\bar{x}_d = \int_{-\infty}^{\infty} dy_d \int_{-\infty}^{\infty} dz_d \int_0^{\infty} dx_d$$

This integral can be expressed using error functions, but noting that $\overline{\kappa}_1 \cong \overline{\kappa}_1'$, we get

$$F_d \approx \frac{\pi D^2}{2} \exp\left[-\left|\overline{\kappa}_1 - \overline{\kappa}_1'\right|^2 \frac{D^2}{4} \right] \tag{58}$$

where

$$|\overline{\kappa}_1 - \overline{\kappa}_1'|^2 = k^2 \left(\cos^2\alpha_0 + \cos^2\alpha_0 - 2\cos\alpha_0 \cos\alpha_0' \cos(\psi_0 - \psi_0') \right).$$

We conducted a study on how sensitive equation (51) is to the value of the propagation distance D. We also studied numerically the sensitivity of the power conservation to D. We concluded that the results are not sensitive to the value of D for the examples we studied.

The shadowing function S_2 in (51) includes shadowing for the incident wave at θ_i, for the scattered wave at θ, and for propagation at the angles α_0 and $\alpha_0{}'$. Thus we write

$$S_2 = S\left(\frac{\pi}{2} - \theta_i\right) S\left(\frac{\pi}{2} - \theta\right) (1 - S(\alpha_0)) \left(1 - S(\alpha_0{}')\right) \qquad (59)$$

7. Evaluation of the Cross Section for the Ladder Term

Let us first find the second-order Kirchhoff approximation for the cross section $\alpha_{\theta\theta}^{2+}$ arising from $\langle J_{2+} J_{2+}{}^* \rangle$. We have from (43)

$$\alpha_{\theta\theta}^{2+} = \frac{4\pi}{A} \mathcal{L}\mathcal{L}'^* H_{11}^{(2)} H_{11}^{(2)'^*} I_+^{(2)} \qquad (60)$$

$$I_+^{(2)} = \langle J_{2+} J_{2+}{}^* \rangle$$

We note, first of all, that $\overline{K}_1 \approx \overline{K}_1'$, and therefore we can let

$$H_{11}^{(2)} H_{11}^{(2)'^*} = |H_{11}^{(2)}|^2 \qquad (61)$$

$$(N_{z1} N_{z2})(N_{z1}{}' N_{z2}{}') = (N_{z1} N_{z2})^2$$

However, we cannot let $\overline{\kappa}_1 = \overline{\kappa}_1'$ in (58). Thus the operator $\mathcal{L}'$ operates only on F_d, and other factors in (61) are all evaluated with $\mathcal{L}$.

Let us first perform the integration with respect to $\psi_0{}'$. Noting that $\psi_0 \approx \psi_0{}'$ in (58), we let

$$\cos\left(\psi_0 - \psi_0{}'\right) \approx 1 - \frac{\left(\psi_0 - \psi_0{}'\right)^2}{2} \qquad (62)$$

We then perform the saddle point integration and get

$$\int d\psi_0{}' \exp\left[-\frac{k^2 D^2}{4} \cos\alpha_0 \cos\alpha_0{}' \left(\psi_0 - \psi_0{}'\right)^2\right] \approx \frac{2\sqrt{\pi}}{kD\sqrt{\cos\alpha_0 \cos\alpha_0{}'}} \qquad (63)$$

Next we perform the integration with respect to $\alpha_0{}'$. We have

$$F_2 = \int_{-\pi/2}^{\pi/2} \sqrt{\cos\alpha_0{}'}\, d\alpha_0{}' \exp\left[-\frac{k^2 D^2}{4}\left(\cos\alpha_0 - \cos\alpha_0{}'\right)^2\right] S_2\left(\alpha_0{}'\right) \tag{64}$$

This integral cannot be evaluated using the ordinary saddle point technique since the second derivative in the exponent goes to zero as $\alpha_0 \to 0$. An approximate integration can be done by noting that most contributions come from the region of small α_0 and $\alpha_0{}'$. We let $\cos\alpha_0{}' \approx 1 - \alpha_0{}'^2/2$ and $\cos\alpha_0{}' \approx 1 - \alpha_0{}'^2/2$. Then we get approximately

$$F_2 = \sqrt{\cos\alpha_0}\, S_2\left(\alpha_0\right) \int_{-\infty}^{\infty} d\alpha_0 \exp\left[-\frac{k^2 D^2}{16}\left(\alpha_0{}^2 - \alpha_0{}'^2\right)^2\right] \tag{65}$$

This can be evaluated using [26] (Gradshteyn and Ryzhik, p. 339):

$$\int_0^{\infty} e^{-\mu x^4 - 2\nu x^2} dx = \frac{1}{4}\sqrt{\frac{2\nu}{\mu}} e^{\frac{\nu^2}{2\mu}} K_{\frac{1}{4}}\left[\frac{\nu^2}{2\mu}\right], \quad Re(\mu) > 0 \tag{66}$$

where $\mu = \frac{k^2 D^2}{16}$ and $\nu = -\frac{k^2 D^2}{16}\alpha_0^2$. For small α_0, $\nu^2/(2\mu)$ is small, and we use

$$K_{\frac{1}{4}}(z) \approx \frac{1}{2}\Gamma\left[\frac{1}{4}\right]\left(\frac{2}{z}\right)^{1/4} \tag{67}$$

We then get

$$F_2 = \sqrt{\cos\alpha_0}\, S(\alpha_0)\, 2\,\Gamma\left[\frac{1}{4}\right] \frac{\exp\left[-\frac{k^2 D^2 \alpha_0^4}{32}\right]}{\sqrt{kD}} \tag{68}$$

Finally we get

$$\begin{aligned}
\alpha_{\theta\theta}^{2+} &= 4\pi \int_{-\pi/2}^{\pi/2} \cos\alpha_0 d\alpha_0 \int_{-\pi/2}^{\pi/2} d\psi_0 [\sigma_{11}]^{2+} \\
[\sigma_{11}]^{2+} &= \left(\frac{k}{2\pi}\right)^2 |H_{11}^{(2)}|^2 \frac{\phi_1\phi_2}{(N_{z1}N_{z2})^2} F_l S_2(\alpha_0) \\
F_l &= \left(\frac{\pi D^2}{2}\right) \frac{4\sqrt{\pi}}{(kD)^{3/2}} \Gamma\left[\frac{1}{4}\right] \exp\left[\frac{-k^2 D^2 \alpha_0^4}{32}\right] \\
S_2 &= S\left(\frac{\pi}{2} - \theta_i\right) S\left(\frac{\pi}{2} - \theta\right)\left(1 - S(\alpha_0)\right)^2
\end{aligned} \tag{69}$$

where $H_{11}^{(2)}$ is given in (44), ϕ_1 and ϕ_2 are given in (55) and (56), and $S(\alpha_0)$ is the shadowing function given in (34) with θ_k replaced by α_0.

Using H_{12}, H_{21}, and H_{22} given in (43), we get the second-order ladder Kirchhoff cross sections for $\sigma_{\theta\phi}$, $\sigma_{\phi\theta}$, and $\sigma_{\phi\phi}$. For J_2, we use $\overline{K}_1 = \overline{K}_{1-}$ given in (41), but this is the same as replacing ψ_0 by $(\pi + \psi_0)$ and α_0 by $-\alpha_0$. Therefore the formula (70) is valid using $(\pi + \psi_0)$ in place of ψ_0 and $-\alpha_0$ in place of α_0.

Finally the ladder cross section $\alpha_{\theta\theta}^2$ for the second-order Kirchhoff approximation is given by

$$\sigma_{\theta\theta}^2 = \sigma_{\theta\theta}^{2+} + \sigma_{\theta\theta}^{2-} \tag{70}$$

where $\sigma_{\theta\theta}^{2+}$ is given in (70), and $\sigma_{\theta\theta}^{2-}$ is obtained using $\overline{K}_{1-}$ for $\overline{K}_1$.

8. Evaluation of the Cyclical Term

Let us now consider the cyclical term $\langle J_{2+} J_{2-}{}^* \rangle$. The scattering cross section per unit area is given by

$$\sigma_{11} = 2Re\left[\frac{4\pi}{A}\mathcal{L}\mathcal{L}'^* H_{11}^{(2)} H_{11}^{(2)'^*} I_c^{(2)}\right] \tag{71}$$

where

$$H_{11}^{(2)} = [\theta]^\dagger [H]^{(2)} [\theta_i]$$

$$[H]^{(2)} = [H]_1 [H]_2$$

and $[H]_1$ is evaluated with $\overline{K}$ and $\overline{K}_{1+}$ while $[H]_2$ is evaluated with $\overline{K}_{1+}$ and $\overline{K}_1$. However $H^{(2)\prime}{}_{11}$ is given by

$$H_{11}^{(2)'} = [\theta]^\dagger [H]^{(2)'} [\theta_i] \tag{72}$$

$$[H]^{(2)'} = [H]_1{}' [H]_2{}'$$

and $[H]_1{}'$ is evaluated at $\overline{K}$ and $\overline{K}'_{1-}$ and $[H]_2{}'$ at $\overline{K}'_{1-}$ and $\overline{K}_i$, see Figure 8. $I_c^{(2)}$ is given by

$$I_c^{(2)} = \int\int \frac{d\overline{x}_1 d\overline{x}_2}{N_{1z}N_{2z}} e^{-i\left(\overline{K}-\overline{K}_{1+}\right)\cdot\overline{r}_1 - i\left(\overline{K}_{1+}-\overline{K}_i\right)\cdot\overline{r}_2}$$
$$\times \int\int \frac{d\overline{x}_1' d\overline{x}_2'}{N_{1z}'N_{2z}'} e^{i\left(\overline{K}-\overline{K}_{1-}'\right)\cdot\overline{r}_1' + i\left(\overline{K}_{1-}-\overline{K}_i\right)\cdot\overline{r}_2'}$$
$$\times S_p S_{2c} \tag{73}$$

where N_{1z} is evaluated at $\overline{K}$ and $\overline{K}_{1+}$ and N_{2z} at $\overline{K}_{1+}$ and $\overline{K}_i$. N_{1z}' is evaluated at $\overline{K}$ and $\overline{K}_{1-}$, and N_{2z}' at $\overline{K}_{1-}$ and $\overline{K}_i$. S_p is the propagation shadowing function, and S_{2c} is the angular shadowing function.

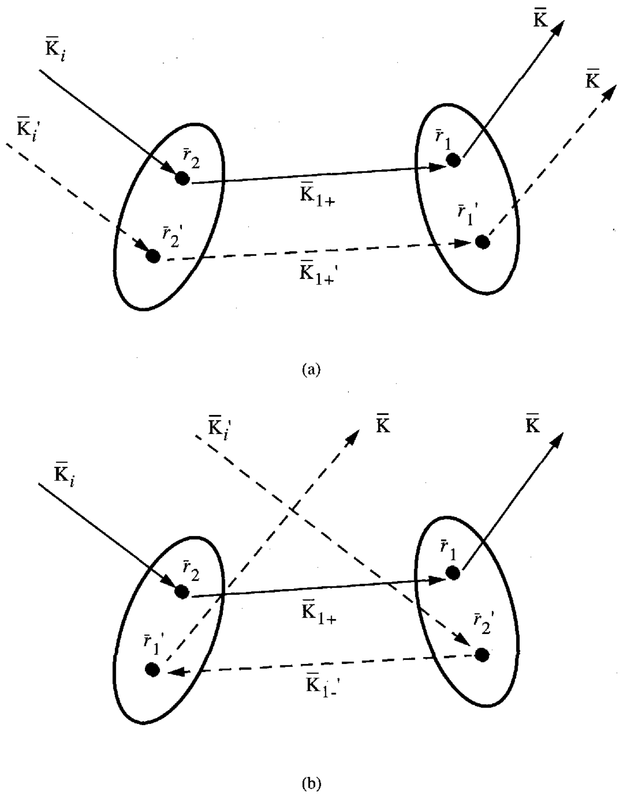

Figure 8. (a) Ladder term $\langle J_{2+}J_{2+}{}^*\rangle$ and (b) cyclical term $\langle J_{2+}J_{2-}{}^*\rangle$. The dashed lines represent the conjugate waves.

Following the procedure in the last section, it is possible to express (73) in the following form:

$$I_c^{(2)} = A\phi_1\phi_2 P \tag{74}$$

where A is the area and

$$\phi_1 = \int \exp -i\frac{1}{2}\left(\overline{\kappa} - \overline{\kappa}_i - \kappa_{1+} + \overline{\kappa}'_{1-}\right) \cdot \overline{x}_{1d} B_1(x_{1d}) d\overline{x}_{1d}$$

$$B_1(x_{1d}) = \langle \exp -i\left(K_z - K_{1z}\right) f_1 + i\left({K_{1z}}' - K_{iz}\right) {f_2}' \rangle$$

$$\phi_2 = \int \exp -i\frac{1}{2}\left(\overline{\kappa} - \overline{\kappa}_i + \overline{\kappa}_{1+} - \overline{\kappa}'_{1-}\right) \cdot \overline{x}_{2d} B_2(x_{2d}) d\overline{x}_{2d}$$

$$B_2(x_{2d}) = \langle \exp -i\left(K_{1z} - K_{iz}\right) f_2 + i\left(K_z - {K_{1z}}'\right) {f_1}' \rangle$$

$$P = \int \exp -i\left(\overline{\kappa} + \overline{\kappa}_i - \overline{\kappa}_{1+} - \overline{\kappa}'_{1-}\right) \cdot \overline{x}_{1d} S_p(x_d) d\overline{x}_d$$

The general expression (73) is now simplified using approximations. First, we note that the two rays with $\overline{\kappa}_{1+}$ and $\overline{\kappa}'_{1-}$ are close, $\overline{\kappa}_{1+} \approx -\overline{\kappa}'_{1-}$, and therefore P is sensitive to the difference between $\overline{\kappa}_{1+}$ and $-\overline{\kappa}'_{1-}$. However, other factors $H_{11}^{(2)}$, ${H_{11}^{(2)}}'^*$, ϕ_1, and ϕ_2 are not sensitive to this difference, and therefore we can evaluate these factors at $\overline{\kappa}_{1+} = -\overline{\kappa}'_{1-}$, and $\mathcal{L}'$ operates only on P. Also we approximate B_1 and B_2 according to the geometric optics approximation used for the ladder term. We also use

$$S_p(x_d) = \exp\left[-\frac{x_d^2}{D^2}\right] \tag{75}$$

Then we obtain

$$\begin{aligned} F_c = \mathcal{L}' P = {} & \frac{\pi D^2}{2} \frac{4\sqrt{\pi}}{(kD)^{3/2}} \Gamma\left[\frac{1}{4}\right] \\ & \exp\left[-\frac{k^2 D^2}{32}\left(\alpha_0^2 + 2(\sin\theta\cos\phi + \sin\theta_i)\right)^2\right] \end{aligned} \tag{76}$$

Finally we get

$$\sigma_{\theta\theta}^{2c} = 8\pi \int_{-\pi/2}^{\pi/2} \cos\alpha_0 \, d\alpha_0 \int_{-\pi/2}^{\pi/2} d\psi_0 [\sigma_{11}]^{2c} \tag{77}$$

$$[\sigma_{11}]^{2c} = \left(\frac{k}{2\pi}\right)^2 \frac{H_{11}^{(2)} H_{11}^{(2)'*} \phi_1 \, \phi_2 \, F_c}{(N_{z1} N_{z2})^2} S_2(\alpha_0)$$

where $H_{11}^{(2)}$ is given in (44) with $\overline{\kappa}_{1+}$, $H_{11}^{(2)'*}$ is given in (44) with $\overline{\kappa}_1 = \overline{\kappa}_{1-} = -\overline{\kappa}_{1+}$, and

$$\phi_1 = \frac{\pi l^2}{\sigma^2 v_{1z} v_{2z}} \exp\left[-\frac{\sigma^2}{2}\left(v_1{}' - v_2{}'\right)^2 - \frac{|\overline{\kappa} - \overline{\kappa}_i - 2\overline{\kappa}_{1+}|^2}{4\sigma^2 v_{1z} v_{2z}{}'}\right]$$

$$\phi_2 = \frac{\pi l^2}{\sigma^2 v_{1z} v_{2z}} \exp\left[-\frac{\sigma^2}{2}\left(v_{2z} - v_{1z}{}'\right)^2 - \frac{|\overline{\kappa} - \overline{\kappa}_i + 2\overline{\kappa}_{1+}|^2}{4\sigma^2 v_{1z}{}' v_{2z}}\right]$$

$$v_{1z} = K_z - K_{1z}{}', \quad v_{2z} = K_{1z} - K_{iz}$$

9. Numerical Examples and Comparison with Millimeter Wave Experiment

The first-order Kirchhoff approximation for the scattering cross section Mueller matrices is given by (19), (16), and (7). The second-order approximation consists of the ladder term for the positive traveling and negative traveling waves given in (70), and the cyclical term given in (77). Numerical calculations are performed for the co-polarized and cross-polarized cross sections in the plane of incidence. In Figure 9(a), numerical examples are shown for TE waves (incident wave in horizontal polarization) for the conducting surfaces ($\sigma = 1\lambda$, $l = 4\lambda$), ($\sigma = 1\lambda$, $l = 3\lambda$), ($\sigma = 1\lambda$, $l = 2\lambda$), and ($\sigma = 1\lambda$, $l = 1.4\lambda$). This is the co-polarized case corresponding to σ_{hh} . Note that the first-order term is significant for ($\sigma = 1\lambda$, $l = 4\lambda$), but as the slope increases, the first-order contribution decreases, and the second-order contribution becomes comparable to the first-order. In Figure 9(b), the cross-polarized case σ_{vh} is shown. Note that the first-order term is zero as expected, and the total cross-polarized cross sections increase with the increase in slope. Note also that the cyclical (cross) terms contribute to the enhanced backscattering, and the enhancement increases with the increase in slope. In Figures 10(a) and 10(b), the co-polarized and cross-polarized cross sections σ_{vv} and σ_{hv} for vertical (TM) incidence are shown for a dielectric surface with relative dielectric constant $7 + i13$. The general shapes of the scattering patterns are similar to those for conducting surfaces; however, the magnitudes are reduced considerably due to transmission and absorption of power into the surface. Figures 11(a) and (b) show the co- and cross-polarized cross sections σ_{hh} and σ_{vh} for horizontal (TE) incidence for the dielectric surface. In Figure 12, experimental data for conducting surfaces are shown for (a) the co-polarized cross section σ_{hh} and (b) the cross-polarized cross section σ_{vh} for horizontal incident polarization and (c) the co-polarized cross section σ_{vv} and (d) the cross-polarized cross section σ_{hv} for vertical incident polarization. Note that as the slope increases, the peaks for the co-polarized cross section shift from specular to backscattering directions, and the cross-polarized cross sections show clear backscattering enhancement.

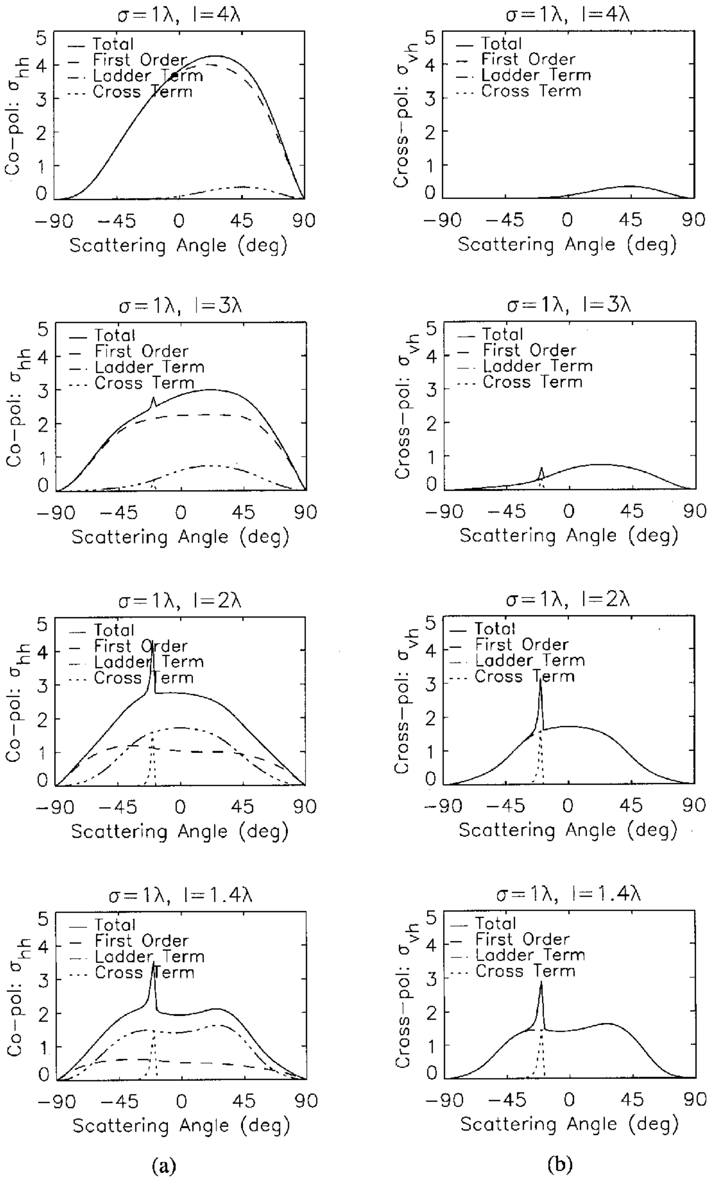

Figure 9. (a) The co-polarized cross section σ_{hh} and (b) the cross-polarized cross section σ_{vh} for horizontal (TE) incident polarization. Plots are for incident angle $\theta_i = 20^\circ$ and conducting rough surfaces. All cross sections are plotted in linear scale.

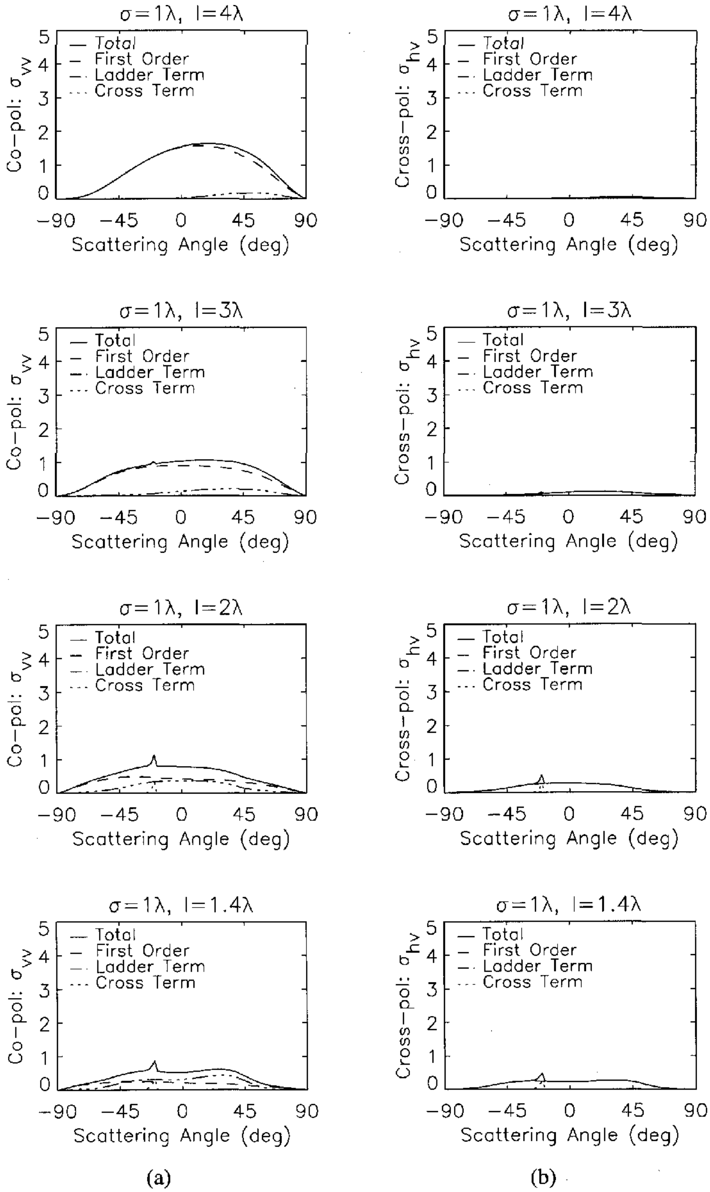

Figure 10. (a) Co-polarized cross section σ_{vv} and (b) cross-polarized cross section σ_{hv} for vertical (TM) incident polaization. Plots are for incident angle $\theta_i = 20^\circ$ and dielectric rough surfaces with relative dielectric permittivity $\varepsilon_{r2} = 7 + i13$

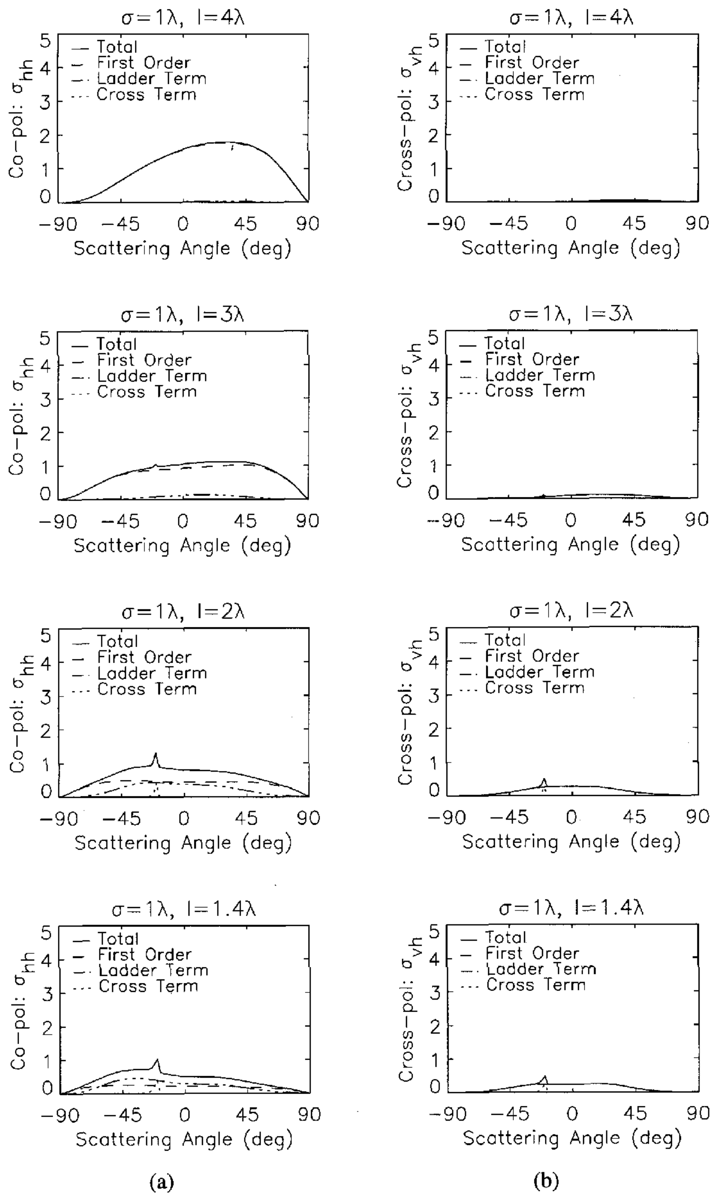

Figure 11. (a) Co-polarized cross section $\sigma_(hh)$ and (b) cross-polarized cross section ${\sigma^0}_{vh}$ for horizontal (TE) incident polarization. Plots are for incident angle $\theta_i = 20^\circ$ and dielectric rough surfaces with relative dielectric permittitivity $\varepsilon_{r2} = 7 + i13$.

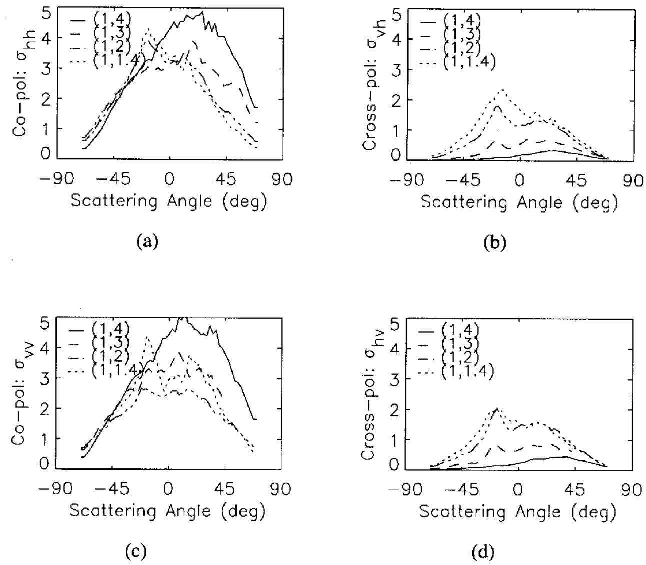

Figure 12. Experimental data (a) for co-polarized cross section σ_{hh} and (b) for cross section σ_{vh} for horizontal (TE) polarization. Experimental data (c) for co-polarized cross section σ_{vv} and (d) for cross-polarized cross section σ_{hv} for vertical (TM) polarization. Plots are for conducting rough surfaces, fabricated using $\lambda = 3mm$ and are averaged over 95-100GHz. The incident angle $\theta_i = 20°$, and the legend refers to (σ, ι) in wavelengths.

Comparison between theoretical calculations and experimental data are shown in Figure 13 for horizontal incident polarization (TE). The data are smoothed with moving averages. Note that agreement is good for the cases ($\sigma = 1\lambda$, $l = 4\lambda$), ($\sigma = 1\lambda$, $l = 3\lambda$), and ($\sigma = 1\lambda$, $l = 2\lambda$). However there are some discrepancies for the high slope case ($\sigma = 1\lambda$, $l = 1.4\lambda$). The difference may be due to the approximations used for the shadowing functions, and this also indicates a limitation of the present theory. Experimental data are obtained using a receiving horn with a field of view of several degrees, which yields averaged experimental data for which any sharp peak within a few degrees is smoothed. Figure 14 shows a comparison between theory and experiment for incident polarization (TM). Note that the analytical results for the TE case are identical to the TM case since the local reflection coefficients are unity under the geometrical optics approximation. In general the analytical theory and experimental data agree well both for magnitude and shape for the region noted in Fig. 1.

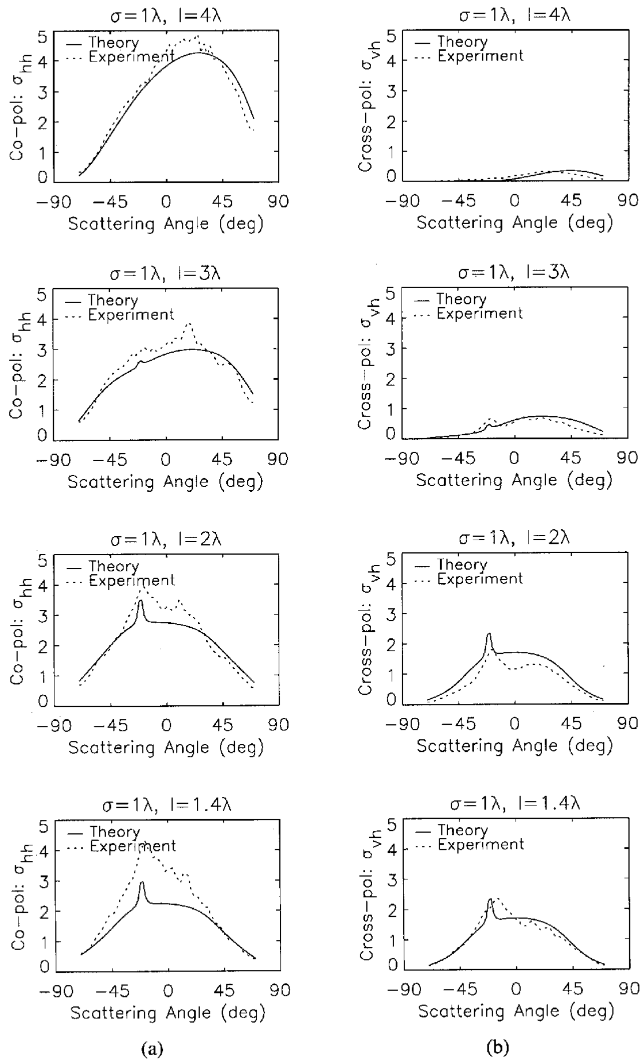

Figure 13. Comparison between theory and experiment. (a) The co-polarized cross section σ_{hh} and (b) the cross-polarized cross section σ_{vh} for horizontal (TE) incident polarization. Plots are for incident angle $\theta_i = 20^\circ$ and conducting rough surfaces. Experimental data are averaged over 95-100GHz, and the surfaces are fabricated using $\lambda = 3mm$.

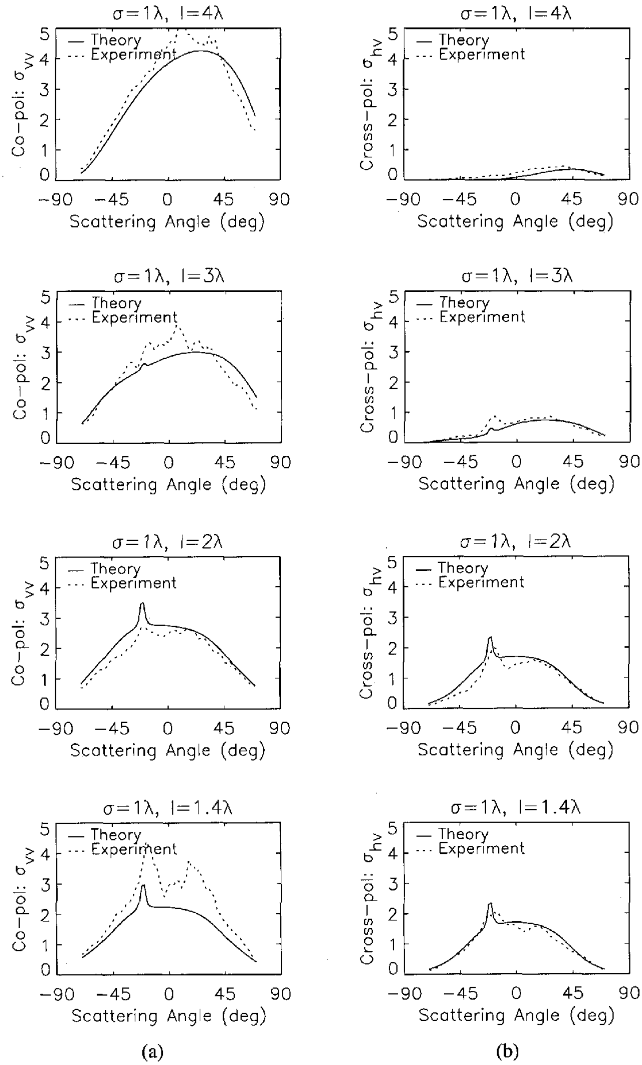

Figure 14. **Comparison between theory and experiment. (a) The co-polarized cross section σ_{vv} and (b) the cross-polarized cross section σ_{hv} for vertical (TM) incident polarization. Plots are for incident angle $\theta_i = 20^\circ$ and conducting rough surfaces. Experimental data are averaged over 95-1000GHz, and the surfaces are fabricated using $\lambda = 3mm$.**

10. Summary and Conclusion

We presented an analytical theory for polarimetric scattering by two-dimensional rough surfaces with an rms slope of order unity. This is the range where backscattering enhancement takes place. Calculated results agree well with millimeter wave experimental data. It should be noted, however, that this theory is based on several approximations. Shadowing corrections are important for accounting for higher order scattering. However, the exact form of the shadowing functions for second-order scattering needs further study. Reduction of the four-fold integrals to double integrals is important in obtaining numerically manageable formulas. However, this reduction involves approximations which could be improved further. We also assumed that the correlation between first- and second-order scattering is negligible. This is reasonable for the geometric optics approximation used here. However, this correlation needs to be included if the theory is to be extended to wider ranges of parameters. The theory is applicable to two media problems. However, if the second medium is lossless,the theory gives poor results because the wave penetrates through one part of the surface and emerges at another part of the surface. In spite of these limitations, the theory gives an approximate formula for the complete Mueller matrix for scattering by two-dimensional rough surfaces and includes backscattering enhancement.

Acknowledgment

This work is supported by the Army Research Office and the National Science Foundation. L. Ailes-Sengers is partially supported by the Clare Boothe Luce Fellowship from the Henry Luce Foundation.

References

1. Ishimaru, A., *Wave Propagation and Scattering in Random Media,* New York, Academic, 1978.
2. Tsang, L., J. A. Kong, and R. T. Shin, *Theory of Microwave Remote Sensing,* New York: Wiley Interscience, 1985.
3. Bass, F. G., and I. M. Fuks, *Wave Scattering from Statistically Rough Surfaces,* Oxford, U.K., Pergamon, 1979.
4. Beckmann, P., and A. Spizzichino, *Scattering of Electromagnetic Waves from Rough Surfaces,* New York, Pergamon, 1963.

5. DeSanto, J. A., and G. S. Brown, "Analytical techniques for multiple scattering from rough surfaces" in *Progress in Optics XXIII,* E. Wolf, Ed. Elsevier Science Publishers B.V., 1986.
6. Nieto-Vesperinas, M., and J. C. Dainty, Ed., *Scattering in Volumes and Surfaces.* Amsterdam, The Netherlands: North–Holland, 1990.
7. Yueh, H. A., R. T. Shin, and J. A. Kong, "Scattering from randomly perturbed periodic and quasiperiodic surfaces" in *Progress in Electromagnetics Research,* J. A. Kong, Ed., New York, Elsevier, 1989.
8. Winebrenner, D. P., and A. Ishimaru, "Application of the phase perturbation technique to randomly rough surfaces," *J. Opt. Soc. Amer.*, Vol. 2, No. 12, 2285–2294, 1985.
9. Broschat, S. L., L. Tsang, A. Ishimaru, and E. I. Thorsos, "A numerical comparison of the phase perturbation technique with the classical field perturbation and Kirchhoff approximations for random rough surface scattering," *J. Electromagnetic Waves and Applications*, Vol. 2, No. 1, 85–102, 1987.
10. O'Donnell, K. A., and E. R. Mendez, "Experimental study of scattering from characterized random surfaces," *J. Opt. Soc. Amer. A,* Vol. 4, 1194–1205, 1987.
11. Nieto-Vesperinas, M., and J. M. Soto-Crespo, "Monte-Carlo simulations for scattering of electromagnetic waves from perfectly conducting random rough surfaces," *Opt. Lett.*, Vol. 12, 979–891, 1987.
12. Celli, V., A. A. Maradudin, A. M. Marvin, and A. R. McGurn, "Some aspects of light scattering from a randomly rough metal surface," *J. Opt. Soc. Amer. A*, Vol. 2, 2225–2239, 1985.
13. Bahar, E., and M. A. Fitzwater, "Enhancement of backscattered diffuse specific intensities from random distributions of finitely conducting particles with rough surfaces," *J. Opt. Soc. Amer.*, Vol. A-5, 89–98, 1988.
14. Fung, A. K., Z. Li, and K. S. Chen, "Backscattering from a randomly rough dielectric surface," *IEEE Trans. Geosci. Remote Sensing,* Vol. 30, No. 2, 356–369, 1992.
15. Ogilvy, J. A., *Theory of Wave Scattering From Random Rough Surfaces,* Bristol: Adam Hilger, 1991.

16. Ishimaru, A., L. Ailes-Sengers, P. Phu, and D. Winebrenner, "Pulse broadening of two-frequency mutual coherence function of the scattered wave from rough surfaces," *Waves in Random Media,* Vol. 4, 139–148, 1994.
17. Ishimaru, A., and J. S. Chen, "Scattering from very rough surfaces based on the modified second-order Kirchhoff approximation with angular and propagation shadowing," *JASA*, Vol. 88, 1877–1883, 1990.
18. Ishimaru, A., and J. S. Chen, "Scattering from very rough metallic and dielectric surfaces: a theory based on the modified Kirchhoff approximation," *Waves in Random Media,* Vol. 1, 21–34, 1991.
19. Phu, P., A. Ishimaru, and Y. Kuga, "Controlled millimeter wave experiments and numerical simulations on the enhanced backscattering from one-dimensional very rough surfaces," *Radio Science,* Vol. 28, No. 4, 533–548, 1993.
20. Ishimaru, A., "Experimental and theoretical studies on enhanced backscattering from scatterers and rough surfaces," in *Scattering in Volumes and Surfaces,* edited by M. Nieto-Vesperinas and J. C. Dainty, Amsterdam: Elsevier Science Publishers, 1990.
21. Ishimaru, A., J. S. Chen, P. Phu and K. Yoshitomi, "Numerical, analytical, and experimental studies of scattering from very rough surfaces and backscattering enhancement," *Waves in Random Media*, Vol. 1, 91–107, 1991.
22. Bennett, J. M., and L. Mattsson, *Introduction to surface roughness and scattering,* Washington, D.C., *Opt. Soc. Amer.,* 1989.
23. Michel, T. R., M. E. Knotts, and K. A. O'Donnell, "Stokes matrix of a one-dimensional perfectly conducting rough surface," *J. Opt. Soc. Amer. A*, Vol. 9, 585–596, 1992.
24. Kim, Y., and E. Rodríguez, "Comparison of the unified perturbation method with two-scale expansion," *IEEE Trans. Geosci. Remote Sensing,* Vol. 30, No. 3, 510–515, 1992.
25. Wagner, R. J., "Shadowing of randomly rough surfaces," *JASA*, Vol. 41, 138–147, 1967.
26. Gradshteyn, I. S., and I. M. Ryzhik, *Tables of integrals, series, and products,* New York, Academic Press, 1980.
27. Phu, P., A. Ishimaru, and Y. Kuga, "Co-polarized and cross-polarized enhanced backscattering from two-dimen- sional very rough surfaces at millimeter wave frequencies," *Radio Science,* Vol. 29, No. 5, 1275–1291, 1994.